STATUS OF EXPERIMENTAL STUDIES OF ELECTRON CLOUD EFFECTS AT THE LOS ALAMOS PROTON STORAGE RING*

R. J. Macek[#,†], A. A.Browman[†], M. J. Borden, D. H. Fitzgerald, R. C. McCrady, T. Spickermann, and T. J. Zaugg, LANSCE Division, LANL, Los Alamos, NM, 87545 USA

Abstract

Various electron cloud effects (ECE) including the two-stream (e-p) instability at the Los Alamos Proton Storage Ring (PSR) have been studied extensively for the past five years with the goal of understanding the phenomena, mitigating the instability and ultimately increasing beam intensity. The specialized diagnostics used in the studies are two types of electron detectors, the retarding field analyzer and the electron sweeping detector, which have been employed to measure characteristics of the electron cloud as functions of time, location in the ring and various influential beam parameters. In addition, a short stripline beam position monitor is used to measure high frequency motion of the beam centroid. Highlights of this research program are summarized along with more detail on recent results obtained since the ECLOUD'02 workshop. Recent work includes a number of parametric studies of the various factors that affect the electron cloud signals, studies of the sources of initial or "seed" electrons, additional observations of electron cloud dissipation after the beam pulse is extracted, studies of the "first pulse instability" issue, more data on electron suppression as a cure for the instability, and observations of the effect of a one-turn weak kick on intense beams in the presence of a significant electron cloud.

INTRODUCTION

Well established electron cloud effects (ECE) at the Los Alamos Proton Storage Ring (PSR) include the two-stream e-p instability, electron-cloud generation by trailing-edge multipactor, and vacuum pressure rise [1-6]. After a brief review of these subjects, the main focus of this paper will be on the results of more recent work on issues regarding e-cloud buildup, some unresolved issues still under study and first results on the beam response to a weak kick.

Two-stream e-p instability at PSR

The fast transverse instability observed since the commissioning of PSR has long been characterized [1] as a two-stream instability arising from the coupled motion of the proton beam and a low energy electron cloud. Some of the most convincing evidence for this conclusion is the observed frequency spectra (modes) for the unstable beam motion near threshold; examples, of which, are shown in Figure 1 for two different beam intensities. The central frequencies for each band occur at the calculated "bounce" frequency for electrons in the space charge potential of the proton beam and vary as the square root of beam intensity. In the coasting beam formula below for the electron bounce frequency, f, N is the number of protons in the ring, a and b the horizontal and vertical half sizes of the beam cross-section, R the mean radius of the ring, r_e the classical radius of the electron and f_e (the fractional neutralization) is the ratio of the electron density to the beam density.

$$\omega_e = Q_e\Omega_0 = 2\pi f = \sqrt{\frac{2Nr_ec^2(1-f_e)}{\pi b(a+b)R}},$$

$$f \approx 230 \text{ MHz } (6.1\,\mu\text{C})$$

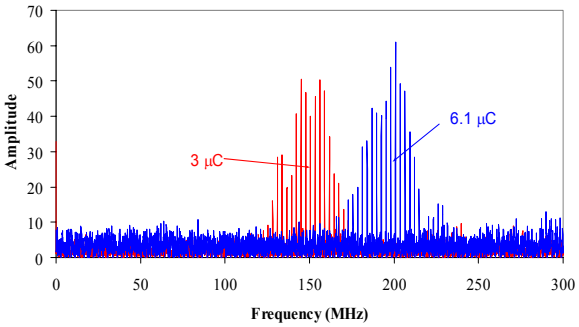

Figure 1. Plot showing the spectra of betatron sidebands from a stripline BPM (vertical difference signal) taken during unstable motion near threshold for two different intensities (6.1 and 3 μC/pulse respectively).

Another important feature of the instability is the threshold behavior plotted in Figure 2.

The definition of the instability threshold used at PSR (for bunched beams with the rf on) is based on an experimental procedure that yields reproducible results at 3-5% of the buncher voltage. A fixed amount of charge is accumulated and stably stored for ~500 μs before extraction. The buncher voltage is slowly lowered until the instability appears near the end of the store as evidenced by the appearance of significant high frequency beam centroid motion on a stripline BPM, accompanied by significant beam loss (~5%) for ~50% of the macropulses.

The linear behavior in Figure 2 is a feature that has been reproduced many times since 1998. Linear behavior is predicted in coasting beam centroid models if the fractional neutralization is constant over the entire range of intensity variation. Since the evidence shown later does not support a constant fractional neutralization, explanation of this behavior is still an open issue.

* Work conducted at the Los Alamos National Laboratory, operated by the University of California for the U.S. Department of Energy under Contract No. W-7405-ENG-36.

[#] macek@lanl.gov

[†] Also affiliated with TechSource, Inc, Santa Fe, NM, 87594

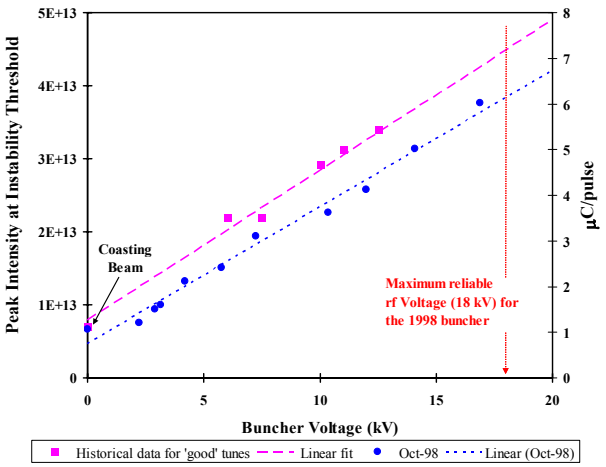

Figure 2. Plot of threshold intensity as a function of rf Buncher Voltage. The square points are historical data for operational beams prior to the direct H^- injection upgrade in 1998 and the blue circles in Oct 1998 after the upgrade.

Control of the instability at PSR has been achieved by various measures which increase Landau damping including higher buncher voltage (more momentum spread), inductive inserts (equivalent to more rf voltage), multipole fields (magnetic sextupoles and octupoles), and coupled Landau damping using a skew quad [2, 3]. There is some evidence that the transverse coupling introduced by vertical closed orbit offsets in sextupoles is responsible for much of the improvement using sextupoles. Mitigation by measures to suppress the electron cloud is more ambiguous and is discussed later in this paper.

Trailing edge multipactor

The origin and characteristics of the electron cloud driving the instability have been key issues in the search for greater understanding of the e-p instability at PSR. Biased collection electrodes were the first diagnostics used to detect electrons in PSR. They provided indications of significant numbers of electrons being generated in some type of avalanche process [7] for beams close to instability threshold but the signals were not easily interpreted. Since then, two types of more suitable detectors have been used successfully to better characterize the electron cloud at PSR. The first is the Harkay-Rosenberg retarding field analyzer (RFA) [8] to which were added fast electronics in order to observe the time structure of the electrons striking the wall [9]. The time information was important for identifying trailing edge multipactor.

Representative samples of the signals from an RFA located in a low-loss straight section (section 4) and for stable beams are shown in the plot of Figure 3. Signals for several values of the repeller voltage are shown in proper time relationship to the beam current signal. The detectors collect electrons striking the wall with energies higher than the value set by the negative repeller voltage, thus providing data on the cumulative energy spectrum, an example of which is plotted in Figure 4.

Relatively "cold" electrons born at the wall (say from beam losses) after the peak of the beam will be accelerated and then decelerated by the beam space charge fields and will strike the wall with some additional energy beyond their initial value. These "multipacting" electrons build up exponentially on the trailing edge of the beam pulse and peak at the end of the beam pulse. In addition to multipactor electrons, electrons captured from the gap at the beginning of the pulse will also be ejected at the end of the bunch. In general, the higher energy electrons appear in a shorter pulse. The signal level at the peak implies ~400-500 μA/cm^2. This is a large flux of electrons, in fact it is 5 orders of magnitude higher than the ~2nA/cm^2 expected from residual gas ionization, assuming that the electrons generated in one passage of the beam pulse emerge in a 40 ns pulse at the end of each beam pulse.

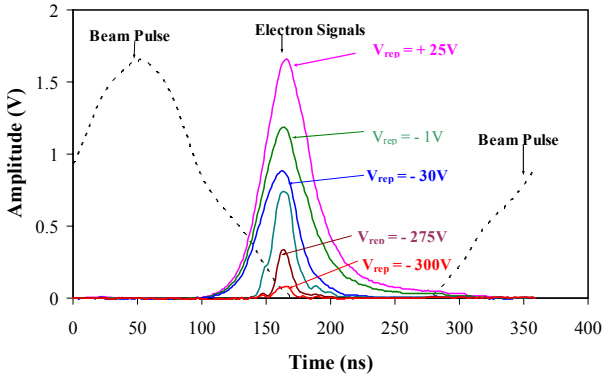

Figure 3. Examples of electrons signals observed with an RFA shown in time relation to the beam pulse.

The electrons signals from the RFA which peak at the end of the bunch are referred to as "prompt" electron signals in contrast to electrons which survive the "gap" between successive passages of the beam bunch.

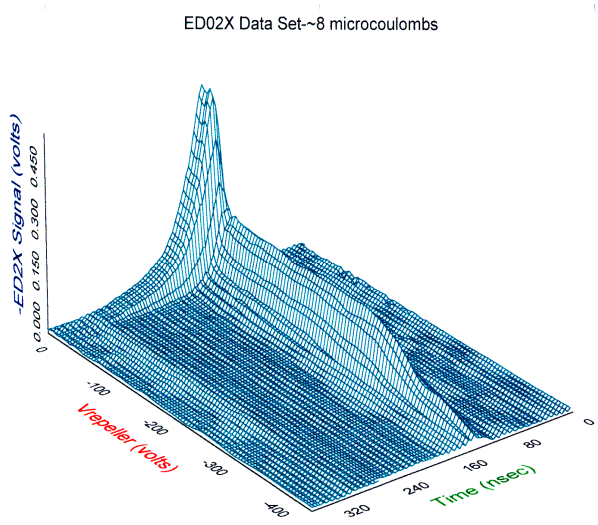

Figure 4. The three-dimensional plot of RFA signals as a function of time and repeller voltage shown here provides a cumulative energy distribution of electrons striking the wall.

Simulations of electron cloud buildup for the long-bunch proton beams of PSR [5, 10] are in good agreement with the shape, timing and energy spectra of prompt (multipactor) signals measured in drift spaces. The amplitude is also in reasonable agreement, given the large uncertainties on the number of seed electrons and the secondary emission yield (SEY) of PSR chamber walls.

Observation of electrons surviving the gap between bunch passages

A key issue for understanding the instability is the number of electrons that survive passage of the gap and are captured by the next beam pulse. The captured electrons oscillate against the protons throughout the pulse and can drive the two-stream instability. Their number is not uniquely determined by the flux striking the wall at the end of the gap. To resolve this issue the electron sweeping diagnostic was developed to measure the number of electrons surviving the gap.

The electron sweeper [9] is basically an RFA with an electrode opposite the RFA opening. The electrode can be pulsed to sweep electrons from the pipe into the RFA. Figure 5 shows signals from the electron sweeper located in a drift space of section 4 of the PSR. The blue curve is the beam pulse. The green is the signal from the collector of the electron sweeper and the red is the high voltage pulse applied to the sweeper. These signals are shown in proper time relation with the beam pulse. Prompt electrons are observed at the end of the beam pulse since the detector functions as a large area RFA until the HV pulse arrives. The "swept" electron signal at the end of the gap is narrow, as expected, and its integral provides a lower limit of ~1 % on the average beam neutralization by the electrons that survive the gap. This is in the range needed to explain the instability threshold in a simple centroid model [1, 3].

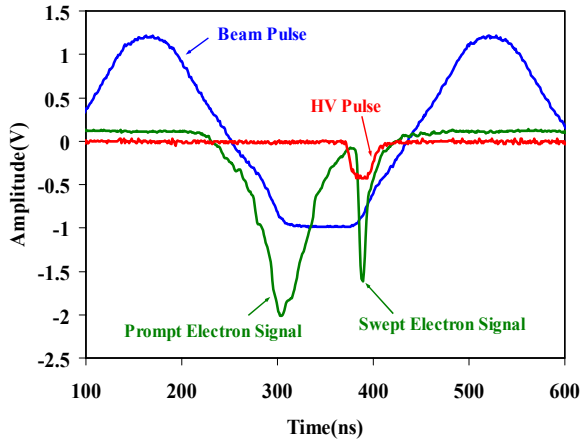

Figure 5. Signal from the electron sweeping diagnostic.

The electron sweeping diagnostic has been used to measure the electrons in the pipe as a function of time after the extraction of the beam pulse from the ring. As can be seen in Figure 6, where both the peak and the integral of the swept electron peak are plotted, either of these signals has a long, approximately exponential tail which is still observable after 1 μs. The decay time constant is ~170 ns and implies a high reflectivity for the low energy electrons left in the pipe. A simple model yields a secondary emission yield (SEY or δ) of ~0.5 for electrons with energies of 2-5 eV (the peak energy of true secondary electrons). Simulations of electron dissipation by Furman and Pivi [10] agree in detail with this data for a value of $\delta(0)$ of ~0.5. This somewhat surprising result is consistent with more recent measurements of SEY down to very low energy incident electrons.

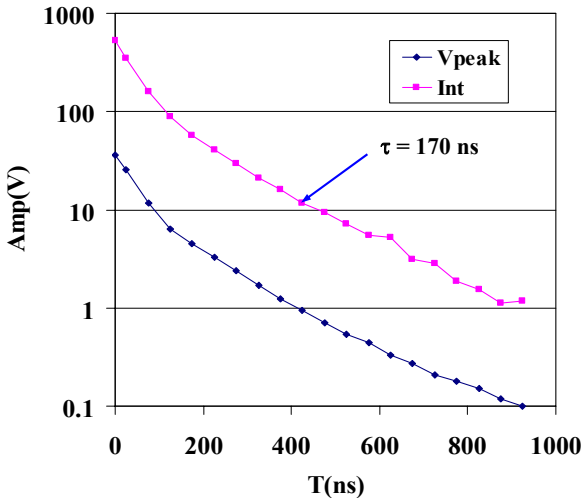

Figure 6. Electron dissipation as measured with the electron sweeping diagnostic.

Parametric studies of electron dissipation decay time (in the region of the approximately exponential tail) over the past 3 years show that it is insensitive to beam intensity, TiN coating, beam scrubbing, location in the ring or location in the extraction line. These observations imply that the SEY for 2-5 eV electrons is insensitive to the same variables.

The electron sweeper was also used to simultaneously measure the prompt and swept electrons as a function of intensity as shown in Figure 7. In this experiment all control variables - buncher voltage, accumulation time, etc - were held constant except the intensity, which, in this example, was varied by moving the stripper foil to control the amount of beam injected.

These plots show that the prompt electron signal varied strongly with intensity as the 10^{th} power over the entire range. The swept electrons measured at the end of the gap varied somewhat more slowly as the 7^{th} power but saturated above 5-6 μC/pulse. This high intensity region is the region of greatest interest for the PSR improvement program and could explain why the threshold intensity doesn't hit a "brick wall" in this region since the fractional beam neutralization from the electrons surviving the gap is roughly constant in the saturation region.

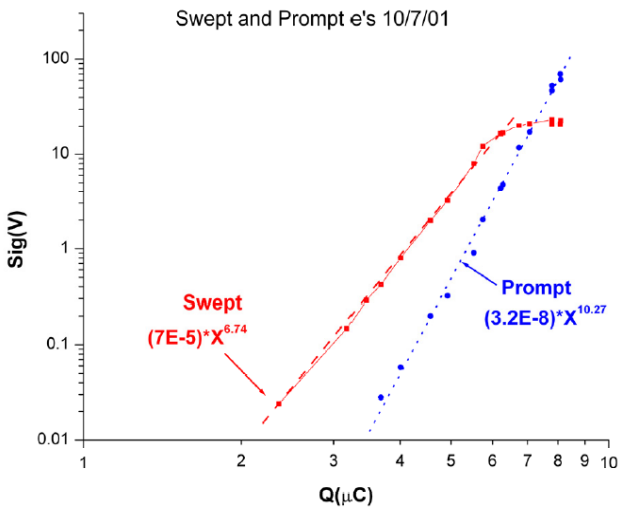

Figure 7. Prompt and swept electrons signal amplitudes plotted as functions of beam intensity (Q).

Saturation of the electrons surviving the gap is presumably due to the space charge forces in the electron cloud in the beam free region. These forces will tend to cause more rapid expansion of the cloud and counter the rapid buildup of electrons fed into the gap by the prompt electrons striking the wall at the end of the bunch.

Vacuum pressure rise

Electron stimulated desorption (ESD) of gas has been observed at PSR for high intensity beams. Gas desorption and vacuum pressure rise are expected consequences of beam-induced multipactor. It was first noticed during beam studies with high peak intensity (>7 μC/pulse) and low repetition rate (1 Hz or less) as a pulsing of the ion pump current meters in synchronism with beam accumulation in the ring. An amplifier (~10 kHz frequency response) was then added to an ion gauge to boost the signal level and allow us to measure vacuum pressure changes on the few ms time scale. A sample signal, shown in Figure 8, was obtained from this "fast ion gauge" for a beam intensity of 8.2 μC/pulse and repetition rate of 0.1 Hz during experiments in May 2000.

The accumulation time for the beam was ~1ms with a store time of 0.3 ms before it was extracted from the ring in a single turn. Sharp noise spikes from the 60 Hz filament supply are visible superimposed on the darker line of ion gauge current. The ion gauge signal has a rise time of ~8 ms which is consistent with the conductance of the aperture to the ion gauge port and a decay time of ~0.5 s which is consistent with the conductance-limited pump down of the 4 inch diameter beam pipe after loading from a short (<1ms) gas pulse. The gas pulse would be produced by ESD from the trailing edge multipactor during the high intensity portion of the beam accumulation and store.

The ion gauge amplifier was calibrated and from the jump in the ion gauge signal during the beam accumulation and store we can calculate a pressure change of $\approx 3 \times 10^{-8}$ Torr. The pressure pulse is a strong function of intensity as is the electron signal. A reduction of about a factor of 4-5 was observed for a beam of 6.7 μC/pulse which is very similar to the reduction in the prompt electron signal in the same section of the ring.

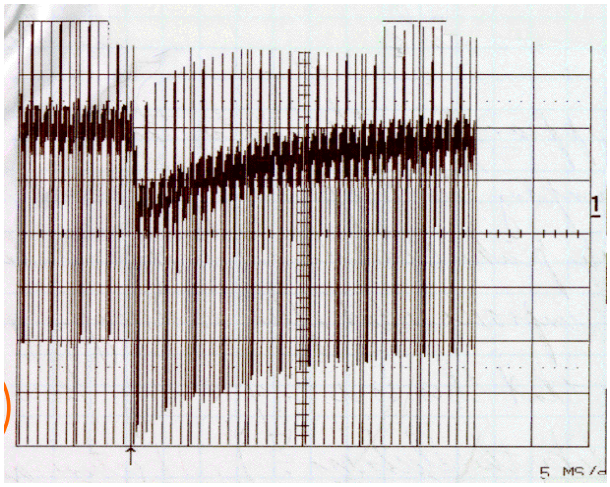

Figure 8. Signal from a modified ion gauge in section 4 of the ring. Time scale is 0.1 s/division.

Comparing the pressure rise to the integral of the flux of electrons striking the wall during accumulation and store (for 8.2 μC/pulse beam intensity) implies about one molecule of gas desorbed per 13 electrons striking the wall. This result also implies an ESD cross-section of $\sim 10^{-17}$ cm^2 for a coverage factor of ~1 (full monolayer) which is in the range published for ESD by ~100 eV electrons [11].

The ion pump currents provide another possible measure of the pressure rise from beam-induced multipactor [2]. We have obtained signals from the ion pumps utilizing the circuit shown in Figure 9. It was designed to be easily moved from pump to pump without modification of any pumps or power supplies.

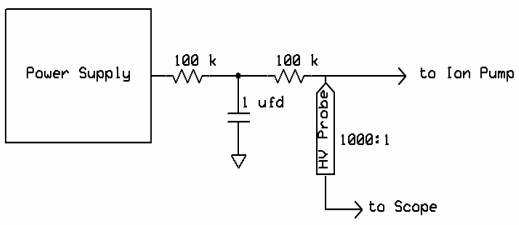

Figure 9. Electronic circuit to measure ion pump currents.

A typical ion pump pulse signal is shown in Figure 10. It was obtained from IP11 in section 1 of the ring during beam studies on 10/04/2003.

The rise time (~0.16 ms) of the ion pump pulse is about the same as the rise time of the integral of a nearby electron detector signal (ED22Y) as shown in Figure 11. The decay time is consistent with the sorption pumping of the pulsed gas load in the interior of the pump (35 liter and internal sorption pumping speed of ~4000 liter/s).

Ion pump pulse signals correlate well with signals from nearby electron detectors with respect to changes in intensity and changes over time from beam scrubbing.

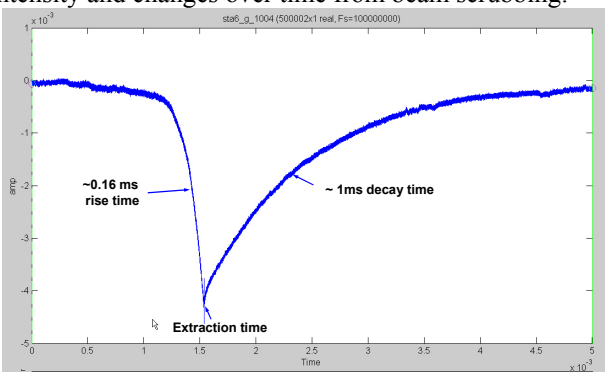

Figure 10. Ion pump pulse obtained during accumulation and 0.1 ms store of a 7.1 μC/pulse beam.

Both the ion pump pulse signals and the prompt electron signals from RFAs are strong functions of beam intensity and vary by the same factor with changes in beam intensity.

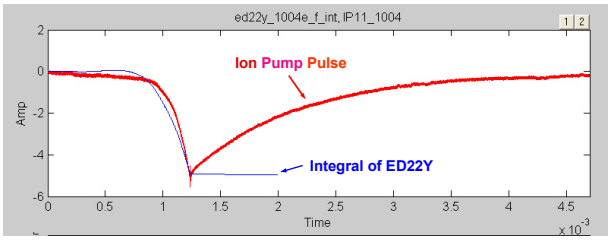

Figure 11. Ion pump pulse (IP11) compared with the integral of the electron signal from the nearest detector (ED22Y).

At this time the mechanism responsible for the observed ion pump signal is not well established. More than one explanation is possible. However, we do find that the signal tracks the signals from nearby RFA electron diagnostics and is thus a simple and useful relative monitor of electron cloud activity.

RECENT STUDIES ON ELECTRON-CLOUD BUILDUP

Parametric Studies

In the past 3 years numerous studies of e-cloud signals have been made to determine the parameters that have the most influence on e-cloud characteristics. Table 1 summarizes the results of the many parameter variations and their effect on the prompt or multipacting electron signal.

As shown earlier (e.g. Figure 7), beam intensity has a strong effect on the multipacting signal. A power law fits the data reasonably well with an exponent that varies from 2-10 depending upon location and amount of beam scrubbing. The effect of added beam in the gap was observed to increase both the prompt electron signal and the electrons surviving the gap. The increase in the latter is consistent with enough additional electrons to neutralize the added beam in the gap. The effect of several other variables will be discussed in later sections.

Table 1. Summary of Parametric Studies

Variable	**Effect on the prompt electron signal**
Beam intensity	Strong effect ~ I^n, n=2-10
Longitudinal bunch profile	Significant effect
Transverse profile	Strong effect, more electrons in direction of major axis
Beam scrubbing	Factor of ~5 reduction over several months
Beam losses	Linear in local losses
Ring vacuum	Linear in local pressure
Location in ring	Significant effect related to other variables at that location
TiN coatings	Mixed results
Weak solenoid field	Factor of ~50 reduction at 20 G
Added beam in gap	Increase in signal and in electrons surviving the gap

Parametric studies of the cumulative energy spectra as functions of intensity, location in the ring, beam scrubbing and TiN have been made but are still being analyzed. Additional observations have been made of electron signals in the presence of sub-threshold coherent motion and some observations for unstable beam. Analyses of these observations are not yet completed.

Source strengths of primary electrons

The primary initial or seed electrons are a crucial input to the simulations. Most simulations have assumed that the dominant source is electrons born at the wall from grazing angle proton beam losses taken as uniform around the ring with 100 electrons per lost proton. The measured beam losses at PSR for ~8 μC/pulse beams imply an average loss rate of $4\text{x}10^{-6}$/proton/turn if taken as uniform around the ring. These parameters are a useful starting point in the absence of better information and yield simulation results in rough agreement with measurements for the drift space of section 4 in PSR. The agreement is fortuitous since the beam losses in PSR are far from uniform around the ring and the angular distribution of beam particles striking the wall near the electron detectors is not measured or simulated.

The 100 e/proton has been justified using the model by Sternglass [12, 13] and is supported by the measurements of Thieberger et al at BNL [14]. In this model, depicted in Figure 12, electrons liberated by energy loss (dE/dx) processes can emerge from the surface if they are produced in the thin, ~1nm, escape zone. This leads to $1/\cos(\theta)$ dependence, which implies that the number of electrons is a very strong function of the grazing angle of incidence. Note that θ is measured from the normal to the surface.

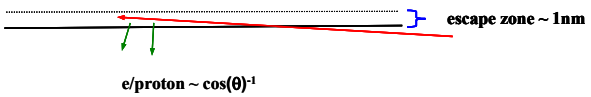

Figure 12. A schematic is shown which illustrates the Sternglass model for electron production from grazing angle interactions of a beam halo particle (red line) with the wall.

Detailed information on the angular distribution for the lost protons incident on the chamber walls near the electron detectors is not available and therefore the 100e/lost proton number is probably best treated as an upper limit. Furthermore, the loss rates can vary by as much as a factor of 1000 at various locations in the ring. Grazing angle losses from foil scattering (largest component of ring losses) occur mainly in the quads and it would be largely secondary particles scattered from the primary loss points that would reach the regions where the various electron detectors are located.

When the information from the local loss monitors is considered, the resulting picture still remains puzzling. A stronger prompt electron signal is consistently observed in section 4 of PSR as compared to sections 2 and 9 where the losses, as measured by local loss monitors or local activation surveys, are an order of magnitude higher. See the Appendix and Figure 28 for a layout of the PSR including the various electron detectors. The ratios of electrons (R_e), local beam losses (R_L) and activation (R_A) with respect to those in section 4 are listed in Table 2. In section 1, where the losses are a factor of 50 higher, the electron signal is only a factor of 6 higher after accounting for the smaller solid angle of the e-detector.

There are several possible explanations for the higher relative electron signals in section 4 of the ring. The local loss monitor or activation data does not provide suitable information on the angular distribution of the radiation striking the walls which could be different in the various sections of the ring. More precise information on the distributions of radiation striking the walls in the vicinity of the various electron detectors is needed before one can know if there is a true discrepancy. Better information on the distributions may be possible from detailed simulation and tracking of lost protons and their secondary products but would require a significant effort to carry out.

Table 2. Ratios of electrons (R_e), local beam losses (R_L) and activation (R_A) with respect to section 4

Section	R_e	R_L	R_A
9	~1/3	~17	7-35
2	~1/2.5	~7	~2
1	~6	~55	~50

The SEY could be different at the locations of the various detectors. It is possible that the higher loss regions were scrubbed at a higher rate. In addition, the vacuum pressure in section 4 was consistently higher than in sections 2 and 9 by a factor of 5-10 and might be responsible for the higher electron signals in that region.

With these issues in mind, a number of experiments were performed where the beam losses and vacuum pressure were systematically varied. Results are presented and discussed in the next two sub-sections.

Primary Electrons from Beam Losses

Beam losses were varied by either moving the stripper foil at injection or by local, closed orbit bumps. Moving the stripper into the beam systematically increased the losses from foil scattering but changed no other beam parameter. Relative changes in the losses were monitored by measuring the foil current which is a measure of foil hits by the stored beam. In the other method, local closed orbit bumps were introduced and relative losses measured with a local loss monitor. In both cases it was found that the electron signals showed significant linear variation with the beam losses as shown in Figures 13 and 14 below.

The equations shown on the graphs of Figures 13-14 are linear fits to the data and R^2 is the "coefficient of determination" for the fit. In Figure 13 the prompt electron signal is plotted as function of changes in beam losses from foil scattering as monitored by the foil current. The intercept at zero foil current is the contribution from the other loss components (primarily excited states of H^0) plus any contribution from the vacuum. The excited states do not change with foil position and so they do not contribute to the slope of the curve.

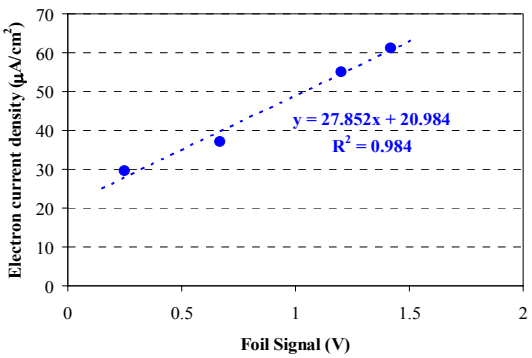

Figure 13. Effect of varying losses (from foil scattering) on the prompt electron signal in drift section 4 for a beam intensity of 5.8 μC/pulse.

Local losses were changed by local horizontal closed orbit bumps (-6 to +8 mm) for the curves plotted in Figure 14. Two identical RFAs were installed at this location, one in the horizontal plane and the other in the vertical plane. Local losses were monitored by a nearby loss monitor, designated as LM59. Here, as in Figure 13, the prompt electrons signals are linear in the losses over the measured range of loss variation. It should be noted that the vertical signal is an order of magnitude larger, presumably due to the larger beam size in the vertical. It is also worth noting that two parameters are changed simultaneously - the losses and the horizontal beam center. The latter could influence the space charge fields and therefore the multipactor "gain".

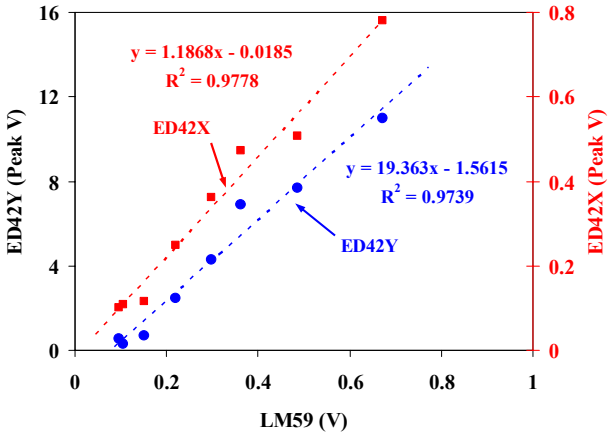

Figure 14. Prompt electron signals from ED42X (detector in the horizontal plane) and ED42Y (detector in the vertical plane) plotted against the variation of local losses produced by horizontal closed orbit bumps in section 4 of PSR. The beam intensity was 8.1 μC/pulse (5×10^{13} protons per pulse).

The sizeable change in electron signals with losses indicates that losses make a significant, possibly dominant, contribution to the primary or seed electron strength. The linear response with losses indicates that the multipactor amplification process has not yet saturated for these conditions. If the multipactor gain could be estimated, say from simulations, then it would be possible to estimate the number of seed electrons from the electron signals. In addition, if the flux of lost particles striking the wall in the vicinity of the electron detectors were known, then it would be possible to estimate the number of seed electrons per lost particle. There is some expectation that the particle tracking code ORBIT [15], under development at ORNL, could be used to simulate both the beam losses and the multipactor signal. Other codes LAHET or MCNPX could be used to simulate the production of secondary products at the proton loss points.

Primary Electrons from Residual Gas Ionization

In the experiment discussed in this section, the vacuum pressure was varied in a number of sections of the ring by turning off ion pumps and monitoring both the pressure and electron signals while the pressure gradually rose. Ion gauges in the drift spaces near the electron detectors monitored the vacuum pressure.

The graph of Figure 15 is one example that illustrates the effect of vacuum pressure on both the prompt and swept electron signals. The vacuum pressure measured by an ion gauge, IG41, in section 4 varied from ~100 nTorr to 2000 nTorr and the prompt signals in these two detectors (ES41Y and ED42Y) increased linearly by approximately a factor of 6 over this range. However, the electrons surviving the gap (swept electrons labeled as ES41Y swept) were unchanged. Other detectors in sections 2 and 5 (ED22Y and ED51Y) gave similar results. Beam intensity was 8.2 μC/pulse (5×10^{13} protons per pulse) during the data collection.

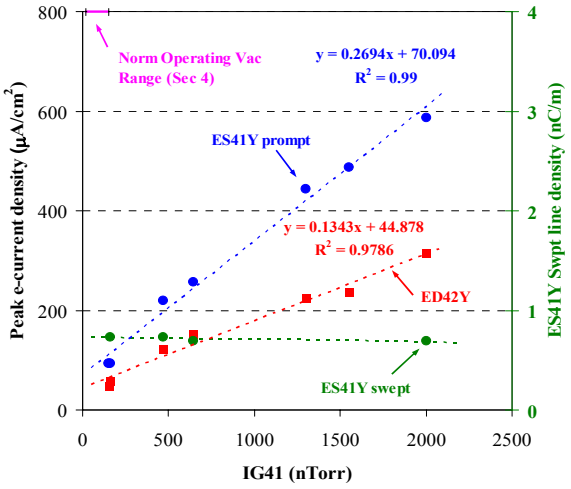

Figure 15. Prompt electron signals (ES41Y and ED42Y) plus the swept electron signal at the end of the gap (ES41Y swept) are plotted as a function of the vacuum pressure in section 4.

From the fits to these curves we can infer that the vacuum contributes 25-30% of the signal in section 4 at 10^{-7} Torr. This section has typically run with somewhat higher pressures than most of the other sections of the ring. The slope of the ES41Y fit is approximately twice that of the ED42Y fit and could be due to a difference in the multipactor gains (from beam size changes) at these locations.

This experiment suggests that residual gas can make a non-negligible contribution to the seed electrons (depending on the actual vacuum pressure). The assumption in most simulations to date has been that residual gas ionization can be neglected because it is small and the electrons are created near the beam not the wall. However, the vacuum effect might be from the ions that are driven to the wall by the beam potential. These hit with as much as 2-3 keV and can release secondary electrons at the wall (~0.3 for 2 keV ions) [16]. To our knowledge, this effect has not yet been included in the published results from simulations.

Suppression of the Electron Cloud Formation

Suppression of the electron cloud build up is widely expected to provide a cure for electron cloud instabilities. Over the years various measures to suppress electrons have been tried at PSR with rather limited results. Initially, various clearing field devices were installed over as much as 15% of the ring circumference [3, 17]. However, it can be argued that these measures were not implemented everywhere in the ring and therefore may have had only a very limited effect on the average electron cloud density.

In recent years, TiN coatings and solenoid windings were tested. Tests of TiN coatings gave mixed results which are tabulated in Table 3 below.

Table 3. Tests of TiN coatings.

Test	Date	Beam Intensity	Prompt electron reduction factor
Section 5	1999	8.5 μC/pulse	>100
Section 9	2002	8 μC/pulse	~ 40
Section 4	2001, 2002	7 μC/pulse	None initially
Section 4 after beam scrubbing*	2002	8 μC/pulse	~5

*After 2 months of operations at 100 μA @20 Hz.

TiN coatings suppressed the prompt signal by a factor of 100 or more for the same beam intensity in our first test in section 5 in 1999 and gave a factor of 40 reduction of the prompt signal in section 9 but provided no improvement in more recent tests in section 4. The TiN coated section 4 has improved with beam scrubbing but only at the same rate as other sections in the ring. The section 4 results are a puzzle since the components were coated at SLAC at the same time as those for section 9. While the section 4 results are disappointing and not understood, one cannot rule out some contamination or compromise of the coated surfaces.

Weak solenoidal magnetic fields suppressed prompt electron signals by a factor ~50 at 20 G [3] in a short section of PSR but when solenoid windings were installed over about 10% of the ring they had no effect on the instability threshold. This suggests that the drift spaces with windings may not be a significant source of electrons that drive the instability.

We have found that beam conditioning (scrubbing) as a result of ongoing beam operations over time reduced the prompt electron signal and improved the instability threshold curves. The first evidence at PSR for the beneficial effects of beam scrubbing on the e-p instability was the repeated observation starting in 1997 that the e-p instability had a lower threshold (~20-30%) during startup after a 4-6 month down period for annual maintenance activities and improved a few weeks later. It was studied more systematically in 2000 as shown in Figure 16 where the threshold intensity is plotted as a function of rf buncher voltage while holding other beam parameters fixed such as accumulation time, bunch length, and injection offset The improvement is rapid at first and slows down after a few days of operation but was still improving after a few weeks of operation at ~100 μA (at 20 Hz). The threshold intensity curves continued to improve into 2001 and 2002 and appear to have stopped improving by late summer of 2002.

In the 2002 run cycle we embarked on a systematic effort to correlate the improvement in instability threshold curves with changes in the electron signals. The two plots in Figures 17 and 18 show the prompt electron signals as functions of time over a several month period in 2002 for an 8 μC/pulse beam.

The data from four electron detectors located in three different sections of the ring is plotted in Figures 17 and 18. ED02X (in horizontal plane) is located 0.6m downstream of the injection stripper foil and ED22Y (in vertical plane) is in the center of the drift space of section 2. ED42Y and ES41Y (both in vertical plane) are both located in the drift space of section 4 and are about 1m apart. Signals from these 4 detectors show a similar factor of 5-10 reduction in signal over this period of time during which PSR operated rather continuously at 100-120 μA at 20 Hz. It should also be mentioned that the swept electron signal (in the drift space of section 4) at the end of the gap showed only a factor of two reduction during this period.

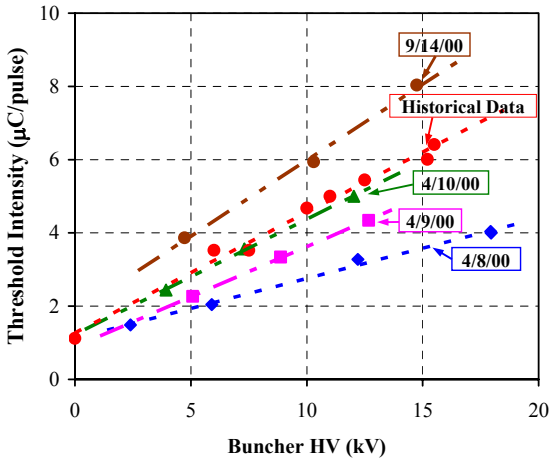

Figure 16. Threshold intensity curves showing the benefit of beam conditioning (scrubbing) during 2000 when there were no inductive inserts in PSR.

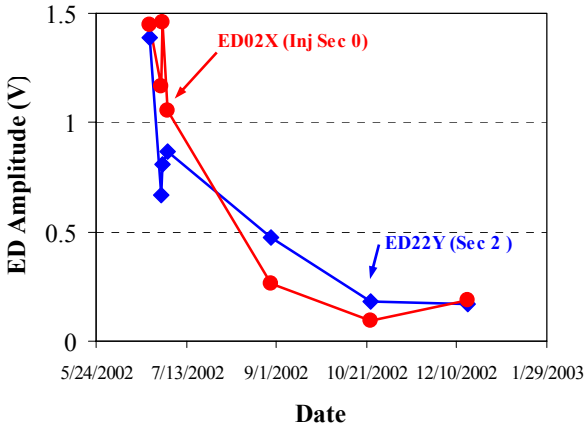

Figure 17. Plot showing the reduction of the prompt electron signal amplitudes for two RFAs (ED02X and ED22Y) during 2002 operations.

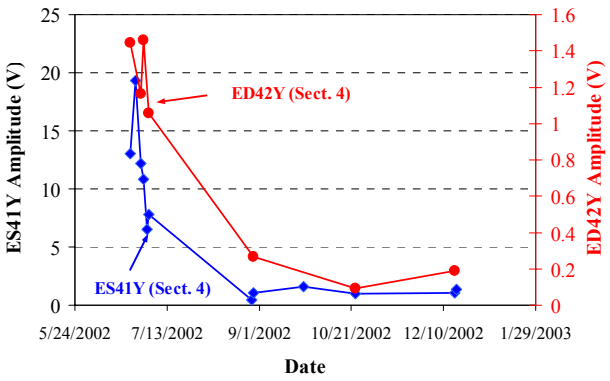

Figure 18. Plot showing the reduction of the prompt electron signal amplitudes for two RFAs (ED42Y and ES41Y in section 4 of the ring) during 2002 operations.

SOME UNRESOLVED ISSUES

Several rather puzzling phenomena which appear to be unique to PSR will be discussed in this section.

Recovery after sweeping the gap

An interesting and not understood effect of sweeping electrons from the gap is shown in Figure 19. The prompt signal following the action of "sweeping the gap" is reduced substantially and takes several turns to recover. Such behavior is not predicted in most PSR simulations to the degree shown in Figure 19.

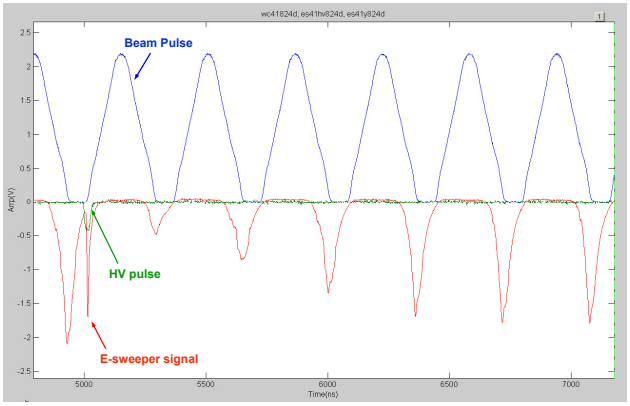

Figure 19. Recovery after sweeping the gap. The red signal is from the electron sweeping diagnostic, the green is the high voltage pulse (500V) applied to the sweeping electrode and the blue signal is the beam current signal from a wall current monitor (WC41) in the ring.

Electrons surviving the gap are captured by the next passage of the beam pulse and will be ejected at the end of the beam pulse and thereby make a contribution to the prompt signal. Sweeping the electrons from the gap means they will be removed from contributing to the next prompt signal. Under this hypothesis, the data implies that the swept electrons account for 75% of the prompt signal and cause the prompt signal to take several turns to build up. We have taken data [18] with the sweeper pulsed every turn for 10 turns with the result that the swept signal has the same amplitude for each of the successive turns. This means the electrons surviving the gap and captured by the beam pulse are not changing after sweeping the gap. Some other mechanism is needed to explain the recovery of the prompt signal.

Electron bursts

Many of the traces shown earlier have been averages over a number (typically 32) of macropulses and don't reveal the turn-to-turn fluctuations. A rather puzzling phenomenon that is not yet understood is the burst character of prompt electron signals shown in Figure 20 for detectors in section 4 of the ring.

The simultaneous traces in Figure 20 cover 110 turns near the end of accumulation. The prompt electron signals vary greatly from turn to turn with some coherence over several turns. The phenomenon varies from day to day and is much more pronounced now than 3 years ago and maybe connected to the gradual decline in strength of the electron signals due to scrubbing of the surface. The electron detector signals in Figure 20 show more fluctuations than are typical in order to illustrate the range of the fluctuations. Another set of traces shown in Figure 21 are more typical of the bursts observed during the past 2-3 years.

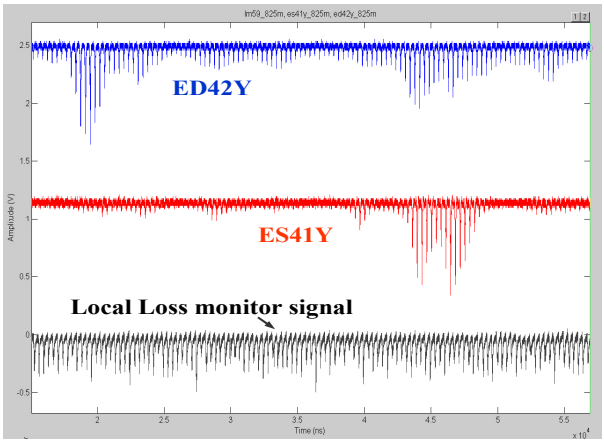

Figure 20. Multi-turn (110) sequence of signals from two electron detectors (ES41Y and ED42Y) and a local loss monitor in section 4 of the ring.

The bursts show no correlation with fluctuations in the local losses but do show some correlation with detectors in other locations around the ring as shown in Figure 21, which suggests that the beam structure somehow causes the bursts. In fact, large increases in the prompt signals and the bursts have been observed when the ring was operated under conditions of low buncher voltage where a microwave-like longitudinal instability introduces ~60 MHz modulation on the beam pulse. The coherence of the bursts over several turns suggests that the betatron oscillations of the beam centroid might be involved. However, no clear correlation with BPM signals has been found. Not all locations show the same levels of fluctuations e.g., the fluctuations near the stripper foil are much lower than those in section 4. Basically the bursts are an unresolved issue. It is hard to claim understanding

of the electron cloud buildup without some reasonable understanding of the cause of the fluctuations.

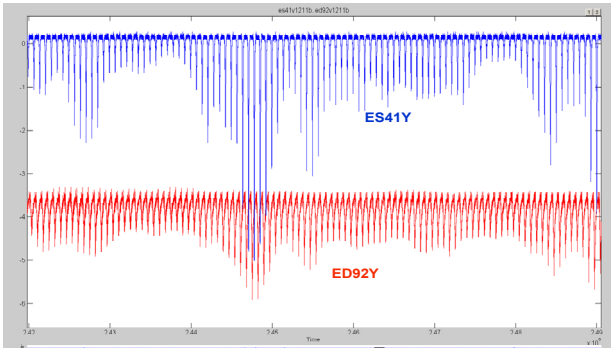

Figure 21. Multi-turn (~100) sequence of signals from two electron detectors (ES41Y and ED92Y) located in section 4 and section 9 respectively.

1st pulse instability

Another curious phenomenon and one that has an adverse impact on single pulse operation of PSR is the so-called 1st pulse instability. As implied by its name, this instability shows up on the 1st pulse in the ring after the beam has been off for the several minutes. We see that the 1st pulse is unstable but subsequent pulses are stable. There is a significant difference in the instability threshold curves for the 1st pulse compared with those for subsequent pulses as shown in Figure 22.

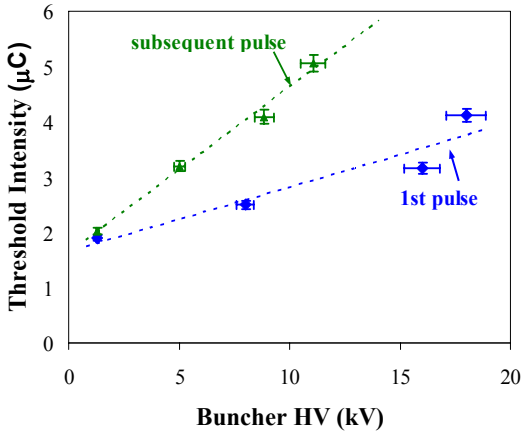

Figure 22. Instability threshold curves for the 1st unstable pulse (blue) and subsequent pulses (green).

The transverse emittance for the beam used for the typical single pulse operation of PSR is about a factor of two smaller than the emittance used for the spallation neutron program at the Lujan center. Such a beam was used during the measurements for Figure 22 but is not required for the 1st pulse instability which is also observed for larger emittance beams.

The 1st pulse instability phenomenon has been observed for several years especially when resuming operations after the annual shutdown for maintenance when the ring has been up to air. The instability disappears after a few weeks of beam operations, presumably due to some sort of beam conditioning. It is interesting that the minimum wait time increases gradually with continual beam operations. Another curious observation is the increased foil current for the 1st pulse compared with succeeding pulse, even for a stable first pulse, as shown in Figure 23. Yet another interesting observation was made by the operators who found that a low intensity precursor (down a factor of 50) generally prevents the 1st pulse instability.

A satisfactory explanation for the 1st pulse instability phenomenon has not yet been developed although there are several ideas (speculations) being offered. The wait time is comparable to the monolayer formation time for the vacuum pressures in the ring, which suggests that adsorption and desorption of gases on vacuum surfaces may be involved.

One hypothesis assumes that certain gases (water?) increase the secondary emission yield, are slow to pump down, and are slowly adsorbed on the vacuum chamber walls during the wait time. The strong electron cloud from beam induced multipacting on the first pulse creates an unstable pulse which further increases the electron bombardment. Gases under electron bombardment are desorbed quickly (a strong pressure pulse is observed on a fast ion pump monitor) and the secondary emission yield is reduced for subsequent pulses. It is difficult to understand how the low intensity precursor pulse would create an electron cloud intense enough to desorb the gas and reduce the SEY sufficient to avoid the instability. The foil current data of Figure 23 and the precursor result suggest that it may be related to gas re-adsorption on the stripper foil. At this time we don't have a plausible model that explains all of the observations.

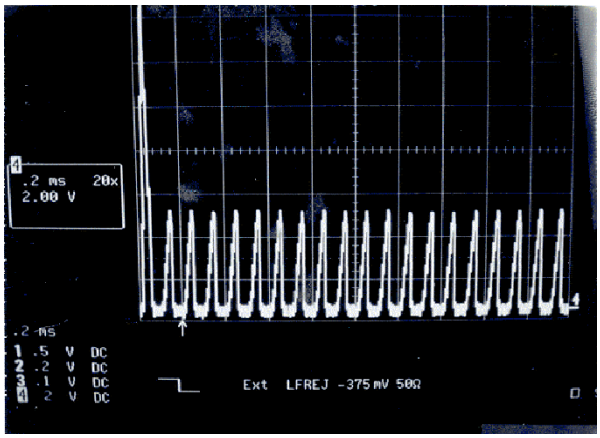

Figure 23. Sequential capture of the foil current signal for 20 consecutive macro pulses after a several minute beam off time.

BEAM RESPONSE TO WEAK KICK

Another interesting set of observations is the beam response to a weak kick. For these experiments we were motivated by the possibility of obtaining information on wake functions/impedance in the presence of an electron cloud through observations of the time-domain analog of beam transfer function measurements. The conditions for the plot shown in Figure 24 are: a beam intensity of 5

μC/pulse and a buncher voltage of 11 kV, a voltage which is twice as large as the instability threshold for this intensity.

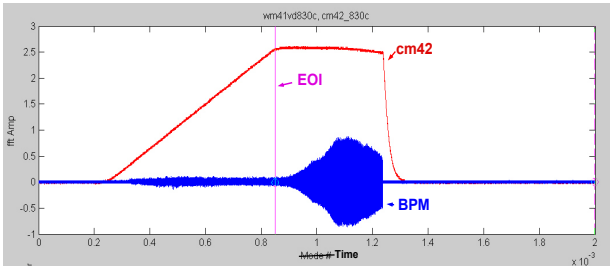

Figure 24. Beam response to a weak one-turn vertical kick applied at the end of injection (EOI). The blue trace is the vertical difference signal from a stripline BPM and the red trace is current monitor (CM42) showing the stored current in the ring during accumulation and a 500 μs store.

It took a surprisingly weak, single-turn kick (1 kV) at the end of injection to elicit a strong beam response at 5 μC/pulse. At lower intensities, 4 times this kick was needed to measure betatron tunes. For the experimental data shown in Figure 24, the beam centroid motion grew to an amplitude sufficient to cause significant beam losses 300-400 μs after the kick. In many ways the response is similar to what is seen in the e-p instability. A spectrogram of the stripline BPM signal is shown in Figure 25 for 500 μs after application of a one-turn kick.

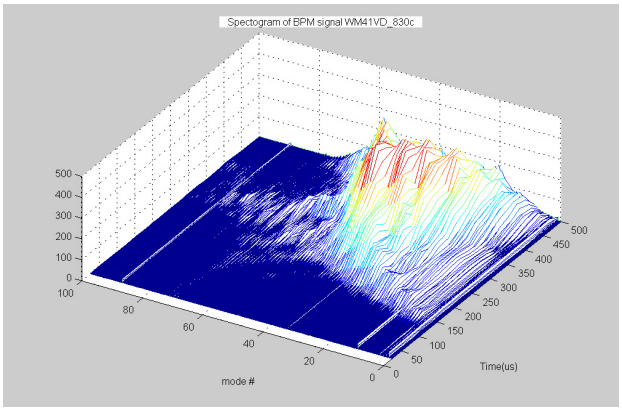

Figure 25. Spectrogram of the BPM signal showing the beam response to a weak kick. The origin of the time axis is the time of application of the one-turn kick. The vertical axis is the fft amplitude of the BPM signal.

The initial response to the kick is a low level betatron oscillation that is barely visible. After ~100 μs or so higher frequency betatron sidebands emerge. They quickly broaden to encompass modes up to ~55, which is somewhat lower than is normal for the standard e-p instability at this intensity. For comparison, Figure 26 shows the spectrogram of the BPM signal for a 5 μC/pulse beam that was unstable (buncher 6.81 kV).

Additional data was collected over a grid of intensity, kick strength and "distance" to the instability threshold in the buncher voltage space. In general, the response is stronger at higher intensity and stronger nearer to the standard e-p threshold. This is as far as we have gone in analyzing the data. In time, we will try to extract wake functions from the data provided the concept proves applicable to the situation with an electron cloud. There are also a few other details that need to be worked out, such as converting the BPM stripline signal to a position signal, before analyzing for wake functions.

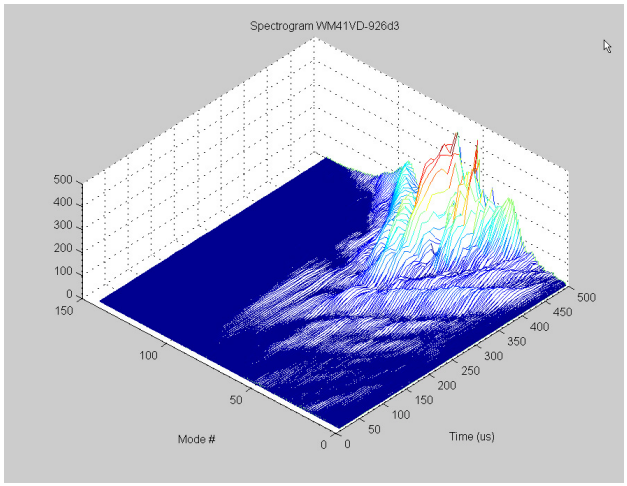

Figure 26. Spectrogram of the BPM signal collected for a 5 μC/pulse unstable beam. The time origin is the end of injection. The vertical axis is the fft amplitude of the BPM signal.

SUMMARY AND CONCLUSIONS

The long-observed two-stream e-p instability is the most serious ECE at PSR and much work has been done to understand its various aspects. The source and characteristics of the electron cloud driving the instability have been long-standing issues and the subject of much beam physics research at PSR in the past several years. Trailing edge multipactor has been shown in experiments and simulations to generate many electrons (at least in the drift spaces) through amplification of primary electrons born near the vacuum chamber walls. The electrons left after the beam pulse passes dissipate more slowly than initially expected with the consequence that a significant number survive the ~100 ns gap between successive passages of the beam bunch. The line density of those surviving the gap (in drift spaces) is about 1% of the average proton beam line density (at ~5 μC/pulse beam intensity). An average line density neutralization of 1% is in the range needed to explain the appearance of the e-p instability in centroid models.

This paper has provided a sampling of results from numerous parametric studies made to identify the control variables having a significant effect on e-cloud signals. Beam intensity was found to have the strongest effect on the prompt (multipacting) electron signals. Beam profile shape, both longitudinal and transverse, also had a strong effect. The prompt electron signals were found to be linear in beam losses and vacuum pressure up to the highest

intensity studied (8 μC/pulse) indicating that the multipactor amplification process has not saturated at PSR.

The experiments and parameter variations that have been simulated show reasonable agreement between simulations and experiments. More data is available for comparisons but require additional simulations.

The source terms for seed electrons from losses have large uncertainties and could be improved with appropriate beam loss and beam scattering simulations. Primary electrons associated with the residual gas make a non-negligible contribution to the electron signal in some sections of PSR. These may be due to electrons born at the wall from ions driven to the wall by the beam potential.

We have obtained mixed results on methods for suppressing trailing-edge multipactor as a cure for e-p. One of three tests of TiN coatings showed no suppression of the electron cloud while the other two tests showed very encouraging suppression of the multipactor electrons. A test of weak solenoids showed a good suppression (factor of ~ 50) of the prompt electron signal but solenoid windings in drift spaces over ~10% of the ring circumference showed no effect on the instability threshold. On the other hand, beam scrubbing over time has had a noticeable effect on both the strength of the electron cloud in drift spaces and on the instability threshold. These results might be explained if drift spaces are not the dominant source of electrons driving the instability.

We do not yet have reliable electron cloud diagnostics installed in PSR dipoles or quadrupoles and therefore can't rule out these regions as the dominant source(s) of electron clouds that drive the instability. Quadrupoles could be the dominant source for two reasons: grazing angle beam losses are expected to be largest in quadrupoles where the beta functions are largest and electrons can be trapped in the quadrupole fields after the beam passes. Various simulations are not yet in agreement on the importance of multipacting in quadrupoles at PSR.

The beam response to a weak kick is interesting but awaits further analysis. The 1st pulse instability is an unexplained puzzle as are the electrons bursts and the recovery following a sweeper pulse. Other open issues include the linearity of the instability threshold curves, the density of electron clouds in dipoles and quadrupoles and the effectiveness of active damping as a cure for the e-p instability.

PROPOSALS FOR FUTURE WORK

There is no shortage of issues regarding ECE at PSR that would benefit from additional work in theory, simulations and experiments. In addition to continuing to analyze data already collected and continuing to exploit electron cloud diagnostics presently installed, we can identify crucial issues whose resolution would likely have a major impact on our understanding and control of ECE for long bunch proton machines. These would include understanding the cause(s) of the electron bursts, measuring the electron cloud in magnets, especially in quadrupoles, and testing the feasibility of active damping of the e-p instability at PSR.

Electrons in quadrupoles

Electrons in quadrupoles are an unresolved issue for PSR. Simulations by Pivi [19] indicate significant multipacting plus trapping in the quadrupole field after the beam pulse passes. For the same number of seed electrons, he found a prompt signal that is a factor of 5 less than in a drift space. However, the source terms for the seed electrons from grazing angle losses should be considerably larger in the quads. If both of these statements are correct then quadrupoles might be the location of the strongest electron cloud density.

Not all simulations indicate strong multipacting in quadrupoles. Thus, for many reasons, it seems crucial to measure the electron cloud in a PSR quadrupole, especially those electrons that are trapped between bunch passages. A concept for doing this is sketched in Figure 27. Fortunately, we have extra aperture in the PSR quadrupoles where a 17 cm diameter aperture is available but only 10 cm is used for the beam chamber. Thus, we can envisage installing an RFA assembly and a sweeper plate and use the assembly much like the sweeping diagnostic installed in drift spaces.

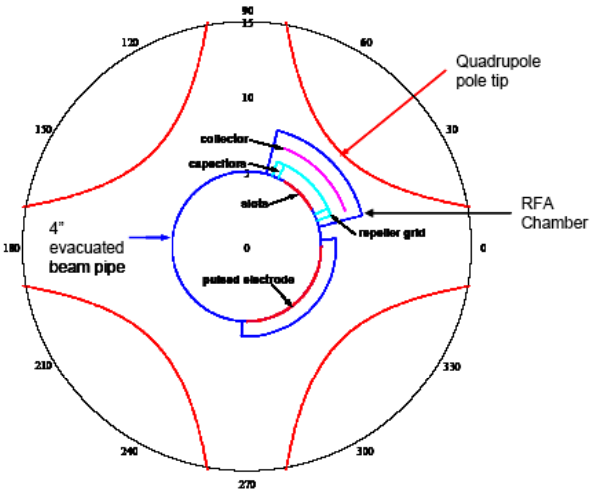

Figure 27. Schematic layout of a proposed electron sweeping diagnostic in a PSR quadrupole.

Active damping of the e-p instability

Active damping is a possible means for controlling the transverse, two-stream e-p instability. The fast growth time and broad frequency content present significant challenges. We are looking at this possibility in collaboration with Professor S.Y. Lee and students at Indiana University and the accelerator physics group (led by Stuart Henderson) at the Spallation Neutron Source (SNS) project at Oak Ridge National Laboratory. The feasibility of a test of the method at PSR is being discussed.

ACKNOWLEDGEMENTS

Robert Macek would like to acknowledge many useful discussions and other collaborative efforts on ECE in the past few years with Miguel Furman, Mauro Pivi, Katharine Harkay, Richard Rosenberg, Robert Kustom, Mike Blaskiewicz, Ron Davidson, Hong Qin, Slava Danilov, Sasha Alexandrov, Jie Wei, Lanfa Wang, Mike Plum, Tai Sen Wang, Paul Channel, S. Y. Lee and Stuart Henderson. All of the authors wish to acknowledge the technical support from the LANSCE-2 and LANSCE-6 groups who maintain, develop and operate the LANSCE accelerator facilities and who made many valuable contributions to the PSR studies reported here.

APPENDIX: PSR LAYOUT

The present layout of the PSR including the various electron cloud and e-p diagnostics referred to in this paper is shown in Figure 28.

Eight hundred MeV H^- beam from the LANSCE Linac is injected into PSR by foil-stripping to protons for 1800-3000 turns. The stripper foil location shown in Figure 28 is just after an H^+, H^- merging magnet in section 0 of the ring. The 10 sections (periods) of the ring are designated sequentially 0 through 9 clockwise around the ring. A cathode follower-based, h=1, rf buncher is used to maintain a beam free-gap in the circulating beam. Extraction from the ring is accomplished in a single turn using stripline kickers in sections 8 and 9.

The numbers after ED or ES labels for electron detectors refer to location. The first digit indicates section and the second digit a sequential location within the section. WM41 is a short (6 inch) stripline BPM used to collect beam position data for unstable beams while WC41 is a wall current monitor with wide band characteristics used to observe longitudinal structure of the beam in the ring. The "pinger" in section 3 is a set of aluminum plates used as an electrostatic kicker and has also been biased as a clearing field or charge collection device.

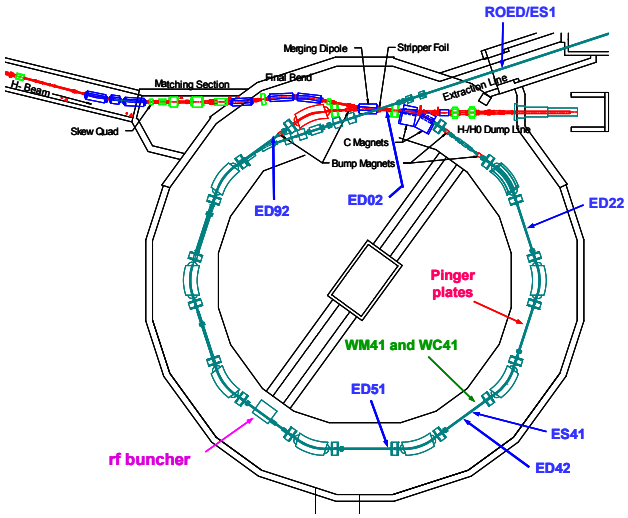

Figure 28. PSR layout including electron detectors and e-p diagnostics.

REFERENCES

[1] D. Neuffer et al, NIM **A321**, p.1-12 (1992).
[2] R. Macek et al, FOAB007, PAC'01, 688 (2001).
[3] R. Macek, ECLOUD'02 Proceedings, CERN-2002-001, 259 (2002).
[4] See contributions to the PRSTAB special collection on Electron Cloud and Two-Stream Interactions in Long-Bunch Proton Beams, at the website: http://prst-ab.aps.org/speced/TwoStreamSC.
[5] A comprehensive collection of recent presentations on ECE at PSR can be found at the Midwest Accelerator Physics collaboration website (3/15-18, e-p feedback collaboration meeting): **http://physics.indiana.edu/~shylee/ap/mwapc/**
[6] M. Blaskiewicz et al, PRSTAB **6** 014203 (2003).
[7] M. Plum et al, RAR23, PAC'95, p. 3406 (1995)
[8] R. Rosenberg and K. Harkay, NIM A **453** p. 507 (2000)
[9] R. J. Macek et al, ROAB03, PAC2003, p. 508 (2003)
[10] M. T. F. Pivi and M. A. Furman, PRSTAB **6** 034201 (2003).
[11] M. J. Drinkwine and D. Lichtman, Progress In Surface Science **8**, pp. 123-142.
[12] E. J. Sternglass, Phys Rev **108**, 1 (1957).
[13] M. Plum, PRS TechNote PSR-95-001 (1995).
[14] P. Thieberger et al, Phys Rev A **61**, 042901 (2000).
[15] J. D. Galambos et al, ORBIT Users Manual, SNS/PRNL/AP Technical Note Number 011, Rev.1.
[16] E. W. Thomas ed., Atomic Data for Fusion, Vol 3: Particle Interactions with Surface, ORNL-6088 (ORNL-6086 V3) (1985), see p. C-4, C-8, and C-12, www.fadc.phy.ornl.gov/redbooks/three/c/c/c.html.
[17] M. Plum et al, PAC'97, p. 1611 (1997).
[18] R. J. Macek, PSR Dev Log Book 98, p. 60 and 63, (9/17/2001).
[19] M. Pivi, private communication to R. Macek, Oct 2003.